CrystEngComm

Accepted Manuscript

ROYAL SOCIETY OF CHEMISTRY

www.rsc.org/crystengcomm

Cite this: DOI: 10.1039/c0xx00000x

www.rsc.org/xxxxxx

COMMUNICATIONS

An innovative glycine complexing approach to silver phosphate myriapods with improved photocatalytic activity

Lili Wang, Na Li, Qiuying Zhang, Sunqi Lou, Yunxuan Zhao, Mindong Chen, Fei Teng*

Received (in XXX, XXX) Xth XXXXXXXXX 20XX, Accepted Xth XXXXXXXXX 20XX
DOI: 10.1039/b000000x

Without using any templates, surface-etched Ag_3PO_4 myriapods are synthesized by a simple glycine complexing method. The unique surface structure endows Ag_3PO_4 with a high specific surface area, thus leading to a greatly improved photocatalytic degradation activity for rhodamine B than solid ones. The glycine complexing strategy is expected to be extended to the preparation of the other photocatalysts.

Semiconductors materials have attracted considerable attention, which are promising to solve current environmental and energy problems. Among them, TiO_2 has been extensively studied due to its low cost, high reactivity and high stability. Owing to its wide band gap, nevertheless, only ultraviolet light can be utilized by TiO_2,[1] which significantly limits its applications in practice. In recent years, silver orthophosphate (Ag_3PO_4) is prevalent because of its high quantum efficiency (up to 90%) in the visible light range.[2] Since the morphology of photocatalysts has a great influence on the photocatalytic and photoelectric properties, numerous efforts have been devoted to the morphology control of Ag_3PO_4.[2-6] For example, Ye and her co-workers have reported Ag_3PO_4 rhombic dodecahedrons,[2] cubes,[2] two-dimensional dendrites[5] and tetrahedrons.[6] Recently, our group is being committed to the study of Ag_3PO_4 and has synthesized Ag_3PO_4 tetrapods[7] and threefold-overlapped Ag_3PO_4 tetrapods.[8] However, it is still a big challenge to acquire Ag_3PO_4 with the novel morphology and the improved photocatalytic activity. To the best of our knowledge, the syntheses of hollow micro/nano structures (e.g., TiO_2,[9] In_2O_3,[10] Bi_2WO_6,[11] Fe_2O_3,[12] etc.) have become an active topic in photocatalysis due to the high surface areas, porous structures and low weights. Compared with solids, hollow ones have greatly improved performances. These hollow structures are usually acquired by the template methods,[9-11] in which the hollow micro/nano structures are mainly predominated by the templates used.[9] The preparations, however, are usually sophisticated and troublesome. It is desirable to develop a simple, innovative method to synthesize the etched structures. Unfortunately, the etched Ag_3PO_4 has not been available in the existing literatures.

In this letter, an innovative, template-free method, for the first time, has been developed for the synthesis of the etched Ag_3PO_4. Typically, the etched Ag_3PO_4 samples were synthesized by a simple precipitation reaction, in which glycine and phosphoric acid were employed as the complexing agent and phosphorus source, respectively. The experimental details of the samples are described in electronic supporting information (ESI Scheme S1).

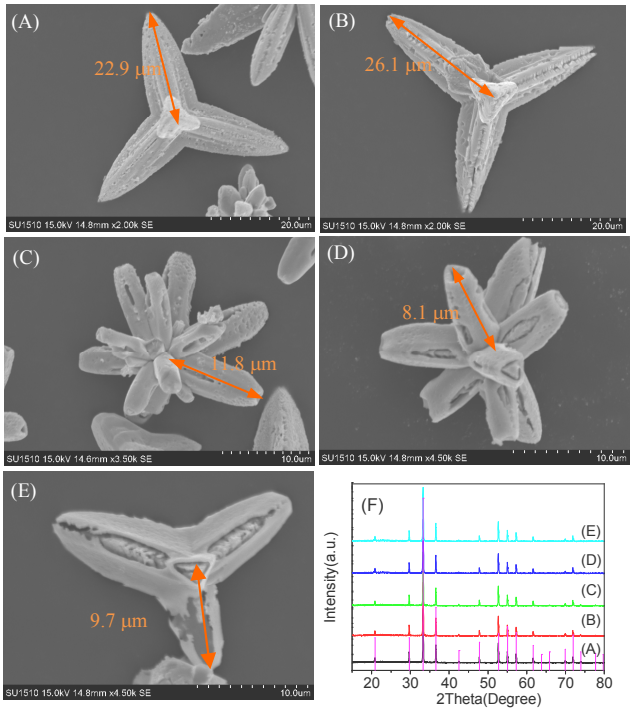

Fig. 1 SEM images (A-E) and XRD patterns (F) of the samples prepared at different molar ratios of glycine/Ag(I): (A) 0.5:1; (B) 1:1; (C) 2:1; (D) 3:1; (E) 4:1. Reaction temperature: 20°C; Stirring time upon adding phosphate acid: 40 min

It was found that the surface morphology and crystal structure of the product were significantly affected by the amount of glycine added, reaction time and reaction temperature. In particularly, glycine was found to be the most vital factor to control the growth of Ag_3PO_4. First, we have investigated the influence of the amount of glycine added on the products. Fig. 1 shows their typical SEM images of the samples, and the size uniformities of the samples can be observed in Fig. S1 (ESI). At glycine/Ag(I)=0.5:1 (molar ratio), the formed particles are solid, only along with a slight erosion of the surfaces (Fig. 1A). Their arms are about 22.9 μm long. At 1:1 (Fig. 1B), not only the surfaces but also the edges of Ag_3PO_4 dendrites are eroded, and even a slight cracking occurs. Besides, its particle size is nearly as large as that of the sample obtained at 0.5:1. At 2:1 and 3:1

(Fig. 1C,D), some holes are produced in the arms, and some cusps disappear. At 4:1, the etched structures spring up (Fig. 1E). It is likely that the erosion first starts from a point on the arm surface, and then gradually expands towards the inners of the crystals. It is obvious that the erosion extent of the crystals is greatly affected by the amount of glycine added. Furthermore, their arm sizes at glycine/Ag(I) =2:1, 3:1, 4:1 are about 10 μm long, which are significantly shorter than those at 0.5:1 and 1:1. With increasing the amount of glycine added, the erosion extent of the sample is becoming more and more evident, and the branch length becomes shorter. This suggests that the crystal growth can be effectively refrained by glycine. Moreover, Fig. 1F shows the XRD patterns of these samples. All diffraction peaks can be well indexed to bulk centre cubic (*bcc*) Ag_3PO_4 (JCPDS No. 06-0505) and no impurities phases are found, confirming the formation of phase-pure Ag_3PO_4.

A plausible formation mechanism is proposed as follows (Equations 1-2):

$$Ag(I) + H_2N—CH_2—COOH \rightarrow Ag(I)\text{-complex} \quad (1)$$

$$Ag(I)\text{-complex} + H_3PO_4 \rightarrow Ag_3PO_4 \quad (2)$$

First, Ag(I) ions are chelated by glycine to form the Ag(I)-glycine complex with a stable constant of 7.76×10^6 [13] and there is a dynamic balance between the ions and complex. Then, a yellow precipitate ($K_{sp}(Ag_3PO_4)=1.4\times10^{-16}$) forms while phosphoric acid is added. After phosphoric acid is added, glycine ions and Ag(I) ions tend to combine with H^+ and PO_4^{3-} from phosphoric acid, respectively. At the glycine/Ag(I) ratio ≤1:1, the free Ag(I) ions will fast combine PO_4^{3-} ions to form Ag_3PO_4. But at >1:1, the spared glycine molecules will exist in the solution; besides, the Ag(I) ions slowly released from Ag(I)-glycine complex slowly react with PO_4^{3-} to form Ag_3PO_4. In the system, glycine molecules also provide a spatial obstacle, reducing the collision reaction of both Ag(I) with $PO4^{3-}$. In that case, the concentration of Ag(I) ions in the solution will increase, preventing ionization of Ag(I) ions from Ag(I)-complex. Then, release rate of Ag ions will reduce, leading to a slow diffusion rate of Ag(I) ions. At a high glycine/Ag(I) ratio, glycine will again combine with Ag(I), resulting a re-crystallization process under hydrothermal condition. Due to the change of releasing rate, the concentration of Ag(I) ions around PO_4^{3-} is definitely different, in which, a concentration gradient is expected to be obvious in the system. Under the conditions, Kirkendall effect [14] may play an important role in the hollowing process. Summarily, the crystal growth is controlled by glycine. Specifically, at a higher molar ratio of glycine to Ag(I) (4:1), the diffusion and releasing rate of Ag(I) ions will become slower and slower and then the concentration gradient around crystals will be smaller and smaller. It will result in each facet growing in parallel. So, the existence of more molecules will lead to the surface growth, other than length growth of arms. The size change in Fig. 1 is a powerful proof. On top of that, the large spatial obstacle in the system favors of the secondary branching growth, leading to the formation of both tetrapods and myriapods. In all, roles that glycine plays in the system can be summarized into two points: the effect of complexing with Ag(I) and a large spatial obstacle it provides.

To further understand the growth process, the time-dependent experiments have been performed (Fig. 2). Once phosphoric acid was added to the solution, the reaction time is recorded. At a

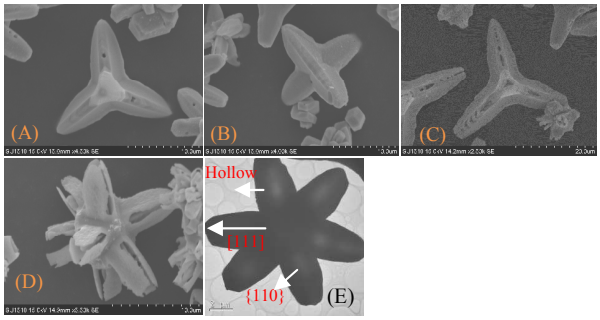

Fig. 2 SEM and TEM images (A-D) of the samples prepared at different stirring times upon adding phosphate acid: (A) 0 min; (B) 15 min; (C) 30 min; (D,E) 40 min. Reaction temperature: 20 °C; glycine/Ag(I) =4:1 (molar ratio)

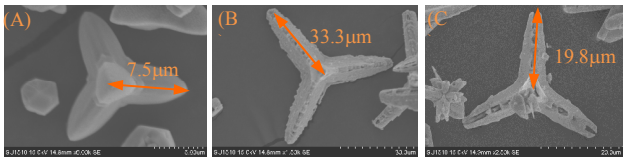

Fig. 3 SEM images (A-C) of the samples prepared at different reaction temperatures: (A) 30 °C; (B) 40 °C; (C) 50 °C. Glycine/Ag(I)=4:1 (molar ratio); Stirring time upon adding phosphate acid: 40 min

time less than 30 min, the erosion of crystals is not obvious, nearly solid. After 30 min, the erosion or even etching occurs obviously. It seems that the erosion process evolves step-by-step. Furthermore, the hollow characteristics can be observed form Fig. 2E, but we can not obtain the lattice fringe images of Ag_3PO_4, because Ag_3PO_4 is fairly unstable under high-energy electron irradiation. Nevertheless, SEM images evidently confirm the presence of etched interiors in Ag_3PO_4 crystals (Fig. 2D). It is found that with prolonging the reaction time, the erosion extent of crystals becomes more severe, but the branch length does not change significantly. Size uniformities of the samples can be observed in Fig. S2 (ESI).

Moreover, the temperature-dependent experiments were performed (Fig. 3). The arm length (33.3 μm, Fig. 3B) of the sample obtained at 40 °C is four times larger than that (7.5 μm, Fig. 3A) of the sample at 30°C. While the arm length (19.8 μm, Fig. 3C) of the sample obtained at 50°C is smaller than that (33.3 μm) of the sample at 40 °C, but is larger than that (7.5 μm) of the sample at 30 °C. It is obvious that with increasing the reaction temperature, the erosion extent of crystals becomes more severe and the branch length becomes longer. It is reasonable that at higher temperatures, the crystals grow faster, thus favoring to form larger crystals; also, the erosion of crystals becomes more severe. Herein, we assume Ostwald ripening is workable not only to size change but also to etching interior.[14,15] During the process of Ostwald ripening, smaller crystals will dissolve and re-crystallize to form larger ones. We attribute the etched structures to the dissolving of central regions and then relocating on the crystal surface. Besides, the pH value of the system was also adjusted by changing phosphorus source: H_3PO_4, NaH_2PO_4 and Na_3PO_4. The details of experiment and results are provided in

ESI (Fig. S3). It is found that a lower pH value contributes to unique surface etching structure, while a higher pH value leads to irregular morphology (Fig. S3, Table 1 of ESI). It is clear that the controllable synthesis of etched Ag_3PO_4 dendrites can be realized under multiple suitable conditions simultaneously.

Furthermore, the degradation of rhodamine B (RhB) is used as a probe reaction to investigate the photocatalytic activity of the etched Ag_3PO_4 under visible light irradiation (λ> 420 nm). The details of activity measurement are provided in ESI (Photocatalytic degradation reactions). From Fig. 4a, the degradation activities of the samples follow the order as follows: 2:1>1:1>4:1>1:2≅3:1. Among, the Ag_3PO_4 samples prepared at 2:1 has the highest degradation efficiency. This may be closely relative to its rough surface although it is not hollow. The rough surface endows the sample with a high BET area, thus improving its degradation activity. From Fig. 4b, the apparent reaction rate constants are calculated to be 0.1077, 0.17794, 0.21103, 0.11575, 0.14656 min^{-1} for glycine/Ag(I) =0.5:1, 1:1 2:1, 3:1, 4:1, respectively. It is obviously that the degradation rate of the samples prepared at 2:1 is twice, 1.4 times, 1.2 times as fast as those at 1:2 or 3:1, 4:1, 1:1. To conclude, small size and rough surface (glycine/Ag(I) =2:1) are good for high degradation. Besides, hollow inside is an important factor that cannot be ignored.

In particular, we further compare the activities of surface-etched Ag_3PO_4 with solid one. Herein, the etched sample was prepared at glycine/Ag(I)=4:1 at 20 ^oC for 40 min, and the preparation details of solid samples are given in ESI. Fig. 5a shows that the degradation efficiency of the hollow sample is three times as high as that of solid one. From Fig. 5b, the apparent reaction rate constants are 0.14703 and 0.0502 for hollow and solid Ag_3PO_4, respectively. It is no wonder that the degradation rate of RhB by the hollow sample is two times higher than that by solid one. Two main factors are attributed to the high activity of hollow Ag_3PO_4: First, the BET areas of etched and solid ones are determined to be 9.2 and 3.1 m^2/g, respectively. The higher BET area can provide more active sites and favors for the adsorption of pollutants on Ag_3PO_4, thus contributing to the improved photocatalytic activity. Second, the intensity ratios of (222)/(110) and (222)/(200) peaks of the etched sample (Fig. 2D) are calculated to be 2.52 and 1.77, which are remarkably higher than those (1.43 and 1.47) of bulk Ag_3PO_4, respectively. This could indicate that the (222) facet grows preferentially for the etched Ag_3PO_4. On base of the previous reports, [2,7,8] we can hold that the etched Ag_3PO_4 mainly expose {110} facets, similar to solid tetrapods and rhombic dodecahedrons. The high-energy {110} exposed facets attribute to the improvement of photocatalytic activity. It is noted that the activity of the etched Ag_3PO_4 dendrites is much higher than our previously reported irregular Ag_3PO_4, the tetrapods and N-doped TiO_2.[7,8] Boldly speaking, the etched Ag_3PO_4 dendrites may be an another big breakthrough step after the rhombic dodecahedron, solid tetrapods, branched dendrites.

Further, electrochemical impedance spectroscopy (EIS) have been conducted to reveal the reason of high photocatalytic activity of etched Ag_3PO_4. Fig.6 presents the Nyquist plots of both solid and etched Ag_3PO_4 (Fig. 5), which are measured in 1 M KNO_3 electrolytes at the open circuit potential of 0.30V *vs*.

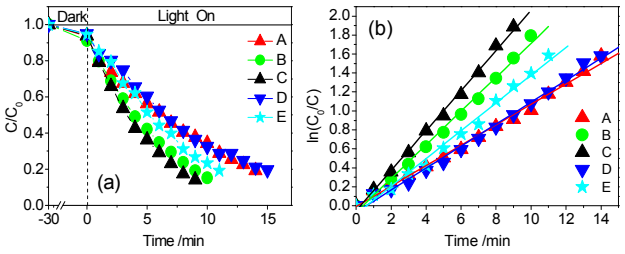

Fig. 4 Photodegradation curves (a) and reaction kinetic curves (b) of rhodamine B (RhB) over the Ag_3PO_4 samples under visible light irradiation (λ > 420 nm): 200 mL 50 mg mL^{-1} RhB; 100 mg of powders, these samples correspond to those in Fig. 1A~E

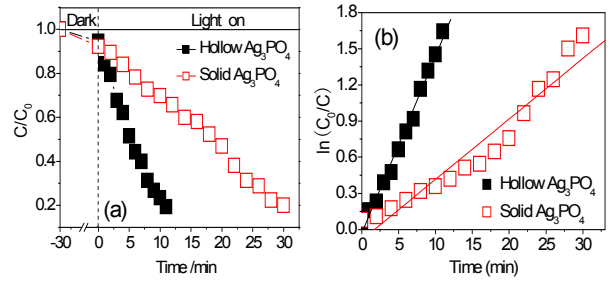

Fig. 5 Photodegradation curves (a) and reaction kinetic curves (b) of RhB over Ag_3PO_4 samples under visible light irradiation (λ > 420 nm): 200 mL 50 mg mL^{-1} RhB; 100 mg of powders; the etched sample is represented in Fig. 2D and solid tetrapods (preparation details are given in ESI 1.3)

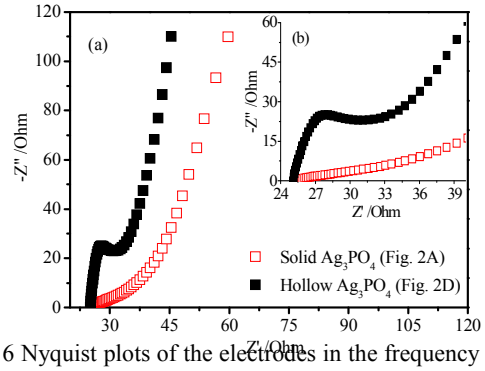

Fig. 6 Nyquist plots of the electrodes in the frequency range from 0.1 Hz to 10 kHz at an open circuit potential of 0.30 V in 1 M KNO_3 aqueous solution: (a) Nyquist plots in the whole frequency range; (b) Nyquist plots in the low frequency range

Hg/HgO in a frequency range of 0.1 Hz to 10 kHz. Both plots are composed of a semicircle and a straight line. From Fig. 6a, we can see Nyquist plots of both samples in the whole frequency range. The semicircle at higher frequency region should be attributed to the charge transfer process at electrode/electrolyte interface, and the straight line at lower frequency region should be ascribed to the diffusion process in solid. The intercept of realpart (Z′) at the beginning of the semicircle represents the internal resistance. In this work, the internal resistance values are almost the same due to the same electrolyte and electrode materials. Fig. 6b further shows that the semicircle of the etched sample is smaller than that of solid one, indicating the charge

transfer resistance of the etched sample is smaller than that of solid one. From the impedance data at lower frequency region, we can observed that at same frequency, the values of the etched sample is higher than those of solid one, meaning that the etched sample has smaller diffusion impedance than the latter. Summarily, the electrochemical property of the etched sample is better than solid one, and its small charge transfer resistance can improve the separation efficiency of the charges. As a result, its photocatalytic performance can be effectively improved.

Besides, charge separation is another factor to improve the photocatalytic activity. Li et al.[16] have reported that photogenerated electrons and holes mainly accumulated on the (101) and (001) facets of titania, and then took part in photocatalytic reduction and oxidation reactions, respectively. They further suggest that the simultaneously exposed two facets can facilitate the charge separation, thus contributing to the improvement of photocatalytic activity. According to Ref.s 2,7 and 8, Ag_3PO_4 dendrites mainly exposed {110} facets, along with minor {111} facets, which may facilitate the charge separation, Limited by our research conditions, however, it is difficult for us to investigate the correlation of exposed facets with charge separation.

Also, we have investigated the cycle stability of Ag_3PO_4. The details of cycle experiment and the results are given in ESI. Fig. S4(a,b) shows that after 14-min reaction, 99.5%, 73% and 50% of RhB has been degraded in the first, second and third cycles, respectively. The catalyst after three cycles is collected to characterize by XRD and SEM (Fig. S4c and d). Its diffraction peaks can be indexed to bulk centre cubic (*bcc*) Ag_3PO_4 (JCPDS No. 06-0505) and Ag (JCPDS No. 04-0783), confirming the formation of Ag_3PO_4 and Ag (Fig. S4c). Under visible light irradiation, Ag_3PO_4 has been reduced to Ag. It is observed from Fig. S4d that neither tetrapods nor myriapods remain present, only fragmented slags form. We have also investigated the cycle stability of solid one (Fig. S4e, ESI). The activity of one are maitained after five cycles for the un-etched Ag_3PO_4. Future research will be carried out to improve its stability.

To conclude, the unique Ag_3PO_4 myriapods can be synthesized by an innovative glycine complexing method. The surface-etched Ag_3PO_4 myriapods show a higher activity than the solid ones, which is mainly attributed to its larger BET area and smaller charge transfer resistance. This work may be an another big breakthrough towards greatly improving photocatalytic properties. It is expected that the glycine complexing strategy will be extended to the preparation of the other photocatalysts.

Acknowledgements

This work is financially supported by National Science Foundation of China (21377060, 21103049), the Key Project of Environmental Protection Program of Jiangsu (2013016, 2012028), the Project Funded by the Science and Technology Infrastructure Program of Jiangsu (BM2013139, 201380277), Six Talent Climax Foundation of Jiangsu (20100292), Jiangsu Science Foundation of China (BK2012862), Jiangsu Province of Academic Scientific Research Industrialization Projects (JHB2012-10, JH10-17), A Project Funded by the Priority Academic Program Development of Jiangsu Higher Education Institutions (PAPD) and Jiangsu Province Innovation Platform for Superiority Subject of Environmental Science and Engineering sponsored by SRF for ROCS, SEM (2013S002) and "333" Outstanding Youth Scientist Foundation of Jiangsu (2011015).

Notes and references

†*The supporting information (SI) can be freely available over the internet of www.rsc.org.*

Jiangsu Engineering and Technology Research Center of Environmental Cleaning Materials (ECM), Jiangsu Key Laboratory of Atmospheric Environment Monitoring and Pollution Control, School of Environmental Sciences and Engineering (AEMPC), Nanjing University of Information Sciences and Technology, Nanjing 210044, China

Corresponding author. Email: tfwd@163.com (F. Teng); Phone/Fax: +86-25-58731090

1. X. Chen, Samuel and S. Mao, *Chem. Rev.*, 2007, **107**, 2891.
2. Y. Bi, S. Ouyang, N. Umezawa, J. Cao and J. Ye, *J. Am. Chem. Soc.*, 2011, **133**, 6490.
3. Y. Bi, H. Hu, Z. Jiao, H. Yu, G. Lu and J. Ye, *Phys. Chem. Chem. Phys.*, 2012, **14**, 14486.
4. Q. Liang, W. Ma, Y. Shi, Z. Li and X. Yang, *CrystEngComm*., 2012, **14**, 2966.
5. H. Liang, X. Xu, W. Chen, B. Xu and Z. Wang, *CrystEngComm*., 2014, **16**, 959.
6. H. Hu, Z. Jiao, H. Yu, G. Lu, J. Ye and Y. Bi, *J. Mater. Chem. A*, 2013, **1**, 2387.
7. J. Wang, F. Teng, M. Chen, J. Xu, Y. Song and X. Zhou, *CrystEngComm*., 2013, **15**, 39.
8. M. Li, M. Chen, J. Wang and F. Teng, *CrystEngComm*., 2014, **16**, 1237.
9. J. Yu, W. Liu, and H. Yu, *Cryst. Growth & Des*., 2008 **8**(3) 930.
10. B. Li, Y. Xie, M. Jing, G. Rong, Y. Tang, and G. Zhang, *Langmuir*, 2006, **22**, 9380.
11. X.-J. Dai, Y.-S. Luo, W.-D. Zhang and S.-Y. Fu, *Dalton Trans.*, 2010, **39**, 3426.
12. L. Li, Y. Chu, Y. Liu, and L. Dong, *J. Phys. Chem. C*, 2007, **111**, 2123.
13. J.A. Dean, *Lange's Handbook of Chemistry* Tab 5-14, 5-15 13th Ed. 1985. 293.
14. H. C. Zeng, *J. Mater. Chem.*, 2011, **21**, 7511-7526.
15. W. Z. Ostwald, *Phys. Chem., Stoechiom. Verwandtschaftsl.*, 1900, **34**, 495
16. X. Wang, R. Li, Q. Xu, H. Han and C. Li, Acta Phys. Chim. Sin., 2013, **29**, 1566-1571.

Graphic abstract

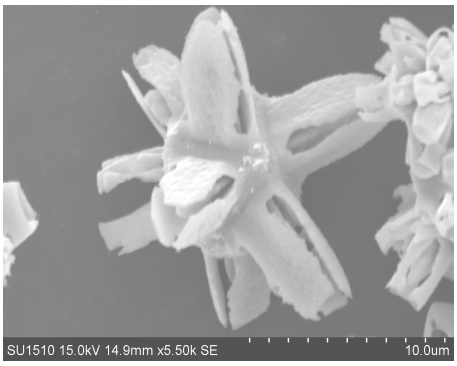

An innovative glycine complexing approach to silver phosphate myriapods with improved photocatalytic activity